JOINT EUROPEAN TORUS

JET–P(89)38

V.P. Bhatnagar, A.Taroni, J.J. Ellis, J. Jacquinot, D.F.H. Start
and JET Team

ICRF Power-Deposition Profiles, Heating and Confinement of Monster-Sawtooth and Peaked-Density Profile Discharges in JET

ICRF Power-Deposition Profiles, Heating and Confinement of Monster-Sawtooth and Peaked-Density Profile Discharges in JET

V.P. Bhatnagar, A.Taroni, J.J. Ellis, J. Jacquinot, D.F.H. Start
and JET Team*

JET-Joint Undertaking, Culham Science Centre, OX14 3DB, Abingdon, UK

** See Appendix 1*

Preprint of Paper to be submitted for publication in
Plasma Physics and Controlled Fusion

Table of Contents

Abstract

The ion-cyclotron resonance heating of monster sawtooth (period greater than the energy-confinement time) and pellet-fueled peaked-density profile in limiter discharges of JET tokamak are studied. The monster sawtooth is a characteristic JET regime which is related to fast ions generated during the minority ion heating. In this regime, the global energy confinement is improved by about 20 % over the sawteething discharges. In the ICRF heating of peaked-density profile discharges, we find typically that T_{i0} is higher roughly by a factor of 2 and T_{e0} roughly by 35 % at a fixed P_{TOT}/n_{e0} when compared to non-peaked profile cases. Also, on a similar comparison, the neutron production rate is found to be higher roughly by a factor of 4. Here, T_{e0} and T_{i0} are central electron and ion temperatures respectively, n_{e0} is the central electron density and P_{TOT} is the total input power. The central confinement improves significantly whereas there is about 20% improvement in global electron kinetic-energy confinement. The ion heating is improved in the pellet case, in part, due to a higher collisionality between the background ions and the energetic minority, but more significantly by a reduction of local ion-energy transport in the central region. Full ray-tracing calculations of power transferred to electrons and ions are consistent with the rate of rise of T_{e0} and T_{i0} in peaked-profile cases. The transport-code simulation of these discharges reveals that there is a reduction of both χ_e and χ_i in the central region of the plasma in the ICRF heated peaked-profile discharges where χ_e and χ_i are the electron and ion heat conductivities respectively. The improvement of confinement is not explained quantitatively by any of the existing η_i-driven turbulence theories as the η_i-parameter ($\eta_i = d \ln T_i / d \ln n_i$ where T_i is the ion temperature and n_i is the ion density) instead of dropping below the critical value remains above it for most of the duration of the improved confinement phase. Understanding of the physical mechanism(s) that play a role in this improvement is not yet clear.

1.0 INTRODUCTION :

The ion-cyclotron resonance heating (ICRH) of JET tokamak has demonstrated, (Jacquinot et al, 1988) among other results, (a) that the plasma can undergo a transition to a new regime, the socalled 'monster sawtooth' (Campbell et al, 1988) in which the plasma enjoys long quiescent periods where there is little coherent MHD activity and the sawtooth instability is suppressed for durations of up to 3 s and, (b) that the pellet-produced peaked-density profiles can be reheated (Jacquinot et al, 1988 ; Schmidt et al, 1988), and sustained for up to 1.2 s resulting in high values of central electron and ion temperatures simultaneously and leading to an increased nuclear reactivity of the plasma.

The former regime, the point (a) above, follows from a growing interest in stablizing the sawtooth instability as it has been recognised that sawtooth activity limits the fusion reactivity of the plasma core and that at a sawtooth collapse, fast particles are lost from the center of the plasma which is a significant energy loss. The minority ICRF heating produces a strong anisotropic minority-ion tail which is well confined in JET. It is believed (Pegoraro et al 1988; White et al, 1988) that this energetic trapped-ion population permits the stabilization of the ideal internal-kink mode as long as the average toroidal precession rate of the particles is greater than the mode growth-rate. In the context of sawtooth stabilization, the minority ICRF heating possesses inherent qualities to produce long sawtooth-free periods in JET plasmas.

The latter regime, the point (b) above, follows from the interest in improving the central energy confinement of a tokamak plasma. It has been argued (Furth, 1986) that introducing a density hump in the center of the plasma (peaked-density profile), such as that produced by a pellet injection, but maintaining at the same time the electron-temperature profile relatively broad so that the current-density profile is resistive-kink stable, would leave the power outflow unchanged and would lead to increased confinement. Another hypothesis that endeavours to predict improved confinement in such discharges, see for example, (Coppi et al, 1978; Horton, 1981; Lee and Diamond, 1986; Romanelli et al, 1986; Dominguez and Waltz, 1987; Romanelli and Briguglio, 1988) is the stabilisation of the socalled η_i-mode (which is essentially an ion-acoustic wave driven unstable by ion temperature gradients where $\eta_i = d \ln T_i / d \ln n_i$). Such a configuration of producing peaked-profile has been tried and attempts to study them with or without additional heating has been made on a number of tokamaks, for example, ALCATOR (Greenwald et al, 1985), TFTR supershots by neutral-beam injection heating (NBI) (Goldston, 1986) and ASDEX (Gruber et al, 1988) etc., with a certain degree of success in achieving improved ion-confinement particularly in high collisionality devices. The improved ion

transport in some of these devices was believed to be consistent with the predictions of the above η_i-driven turbulence theory.

In the JET experiment, the peaked-density profiles were obtained by pellet injection and, for the first time, these peaked profiles were reheated with high-power ($\approx$12 MW) minority ion-cyclotron resonance heating. The ICRF heating is well suited for this purpose, as it can deposit RF-power centrally in a high-density plasma with a relative ease as compared to other methods such as, for example, NBI.

In this paper, we compare experimental results of electron and ion-heating in discharges that feature monster sawtooth with those in pellet-produced peaked-density profile discharges which were heated with ICRF. Also we carry out a comprehensive analysis of ICRF-heated peaked-density profile discharges by a transport code JETTO (Cenacchi and Taroni, 1988) to simulate the evolution of JET discharges and to provide an insight into the improved heating and confinement found in these discharges. In this analysis, the ICRF power-deposition profile in the minority-heating scenario is computed by an RF package based on the ray-tracing code BRAYCO (Bhatnagar et al, 1984). Such a transport-code simulation of these discharges reveals that there is a reduction of both χ_e and χ_i in the central region of the plasma in the ICRF heated peaked-profile discharges. But, identification of the physical mechanism(s) that play a role in this improvement has not yet been fully understood (for a discussion see Section 4). A similar analysis has also been carried out by Hammett (Hammett et al, 1989) using TRANSP-code, and by Milora (Milora et al, 1989) using WHIST-code for similar JET-discharges (see also Bhatnagar et al, 1989a).

The paper is organised as follows. In section 2, we illustrate the ICRH produced 'giant' and 'monster' sawteeth and present the electron and ion heating in such discharges with a specific view to establishing a basis for evaluation of the gain represented by peaked-profile discharges. The results of heating and confinement in the peaked-density profile discharges are then compared with the above giant and monster sawteeth discharges. In Section 3, we concentrate on the analysis of the ICRF heated peaked-profile discharges by simulating the evolution of two representative discharges by a transport-code in which the ICRF power deposited in electrons and ions is calculated by an RF-package based on ray-tracing. Discussion and conclusions of this study are contained in Section 4.

2.0 EXPERIMENTAL RESULTS :

JET (Joint European Torus) is a D-shaped large tokamak (Rebut et al, 1984) with major radius R_0 = 2.96 m, minor radius a_p = 1.2 m, nominal toroidal field B_t = 3.4 T, plasma current I_p = 5 MA (upgraded to 7 MA), and plasma elongation = 1.6. For the results presented in this paper, we include the ICRH data obtained in JET limiter discharges that produced giant and/or monster sawteeth for I_p varying from 2 to 6 MA (Bhatnagar et al, 1989b). The plasma composition was hydrogen minority ($\approx$ 5-10%) in deuterium or helium majority gas. This data is then compared with ICRF heating of peaked-density profiles produced by pellet injection and it pertains to I_p = 3 MA. In these discharges deuterium pellets were injected in deuterium majority gas at the end of the rise of plasma current before the discharge starts sawteething. In some shots minority gas was hydrogen whereas in others it was helium-3. Helium-3 minority case allows to study (see also Section 4) the ICRF heating of a discharge where no direct ion-heating occurs via the second-harmonic resonance in contrast to the hydrogen minority case where deuterium second-harmonic is degenerate with the hydrogen fundamental resonance. Some shots with pellets also had neutral-beam injection ($P_{NB}/P_{RF} \approx 0.25$) for diagnostic purposes to measure the ion-temperature by charge-exchange recombination (CXR) spectroscopy. For general tokamak diagnostic systems including that of JET see, for example, a review paper (Orlinskij and Magyar, 1988 and references therein). In the data presented here, the electron-temperature profile was measured by the usual electron-cyclotron emission diagnostics and the ion-temperature in the central region was routinely measured by Doppler broadening of Ni-XXVII spectral-line by a high-resolution X-ray crystal spectroscopy technique . The electron density and its profile was measured by a multi-channel far infra-red interferometer. The peaking of the electron density and temperature profiles is also verified by a LIDAR (LIght Detection And Ranging) Thomson scattering system at some fixed time-slices.

The JET ICRH system has been described previously (Wade,1985 ; Kaye, 1987). In the early ICRH experiments (1985-86) on JET, three (A_{01},A_{02}) antennas (see Wade, 1985) located on the low-field side of the tokamak were used. These have been replaced by eight A_1 antennas (see Kaye, 1987) which are symmetrically distributed around the torus. A JET antenna has essentially two radiating elements that are separated toroidally which can be driven in phase (monopole) or out of phase (dipole). In monopole operation, the antenna radiated power spectrum is centered at k// = 0 with a half width of 4.5 /m whereas in dipole operation k// = 7 /m and the half width is 3.5 /m. An electrostatic screen made out of nickel (which in future experiments will be replaced by Beryllium) is used to filter out the slow wave. ICRH power is delivered to the plasma by coupling the fast magnetosonic wave which deposits its power mainly via the

minority-ion cyclotron damping in a narrow region (about 30 cm) near the ion-ion hybrid resonance zone (Jacquinot, 1986).

In JET, peaked-density profiles are produced by pellet fueling in the current ramp-up phase of the discharge and are followed by heating by ICRH and/or neutral beam injection (NBI) in limiter discharges. Deuterium pellets of 2.7 and/or 4 mm diameter (nominal speed ≤ 1.5 km/s at a rate of several pellets per second) are injected horizontally into the midplane of the tokamak deep inside the plasma at predetermined times by a multi-barrel, multiple-pellet, pneumatic injector (see Kupschus et al, 1988 and Milora et al, 1988). In ohmic discharges the peaked profiles can be sustained typically for 4-5 s whereas with ICRH, until now, the peaked profile was maintained for up to a maximum of 1.2 s only. In these discharges, ICRF power upto 12 MW was applied and $T_{e0} \approx 11.5$ keV and $T_{i0} \approx 10$ kev was achieved. The range of plasma parameters under ICRF heating with and without pellet injection are given in Table 1.

2.1 Giant and Monster Sawtooth:

The ICRF minority heating generally produces 'giant' sawteeth where $T_{e0}(max)/T_{e0}(min) \cong 2$ compared to 1.1-1.2 in the ohmic phase and the sawtooth period is also increased by a factor of 2-3 (see Fig. 1). The strong electron heating is related to the fact that during ICRH, an energetic (0.5-1 MeV) minority-ion tail is produced which relaxes on the electrons and heats them predominantly. When the ICRF power is centrally deposited and exceeds a certain threshold (which can be in some cases as low as $\cong 3$ MW), monster sawteeth (see Fig. 2) are produced generally when $q_{cyl} \cong 3.3$ and the stabilisation is beleived to be due to the presence of fast ions (Pegoraro et al, 1988; White, 1988). During the stable period, density and stored energy rise slowly but T_e saturates. The reaction rate increases due to peaking of temperature profiles (for other aspects, see Campbell et al, 1988).

2.2 Central Energy Confinement:

For limiter ICRH discharges, we plot, in Fig. 3 and 4, T_{e0} and T_{i0} as a function of P_{TOT}/n_{e0} for a range of plasma currents I_p = 2-6 MA, where the subscript 0 refers to the central values. The data for 2-3 MA is mostly of monster sawtooth whereas for 5-6 MA, it refers to the usual giant sawteeth. For a given 'central confinement-volume', the data in Fig. 3 and 4 can be directly related to central electron and ion kinetic-energy confinement times respectively. A clear off-set linear behaviour (see, for example, Bhatnagar et al, 1989b) is seen in the T_{e0}-plot whereas the T_{i0}-plot tends to saturate. This behaviour is a general characteristic of the ICRF minority-heating and will be compared to the particularly interesting case of peaked-density profile heating (see below). We note that within the scatter of the data there is little difference in the central incremental confinement time for 2-6 MA which has been independently verified by a local analysis (Christiansen et al, 1988).

2.3 *Peaked-Density Profile Heating :*

We present results of peaked-density profiles that are produced by pellet fueling in the current ramp-up phase and are followed by ICRH in JET limiter discharges. Figure 5 shows time traces of RF-power launched, DD-reaction rate (R_{DD}), central electron temperature (T_{e0}), central ion temperature (T_{i0}), volume-average electron density ($<n_e>$) of a 3 MA shot in which a 4 mm pellet penetrates to the center of the plasma and produces $n_{e0} \approx 1 \times 10^{20}$ m^{-3} which slowly decays but the peaked-profile is maintained for 1.2 s. An example of the peaked-density profile produced in such discharges is shown as a 3-dimensional plot in Fig. 6. Due to cooling by the pellet, T_{e0} initially drops but the immediate application of ICRH heats electrons steadily. Initially the T_e-profile is flat but becomes more and more peaked as time evolves. The T_e-peaking factor ($T_{e0} / <T_e>$) remains smaller than the density peaking factor ($n_{e0} / <n_e>$) for a short time but, after about 0.25 s overtakes it and increases steadily. There is a crash at 44.45 s due to an MHD event at which time the peaked-profile disappears and R_{DD}, T_{e0}, T_{i0} all drop though P_{RF} is still maintained. A further account of the investigation of the crash and certain other aspects of peaked-profile discharges can be found elsewhere (Schmidt et al, 1988). Here (see Section 2.4) we concentrate on a comparison of the electron and ion heating of these discharges with those described in Section 2.1.

2.4 *Comparison of Monster-sawtooth and Peaked-Profile Discharges:*

In Fig. 3 and 4, we compare the electron and ion heating of peaked-density profile discharges heated with ICRF with the heating of broad-density profiles obtained both in monster and non-monster sawtooth discharges. We note that T_{e0} is improved by about 35% but, the most important gain is obtained in the ion temperature which is increased by a factor of 2 and allows high T_{e0} and T_{i0} simultaneously which is not achieved otherwise. The comparison shown in Fig. 3 and 4 demonstrates that the central confinement has improved significantly. But, there is only a small improvement when $<T_e>$ is compared at a fixed $P_{TOT} / <n_e>$. By another analysis, we find that with peaked-density profile heating, the global electron kinetic-energy confinement is about 20% better. Also, the neutron production rate in the peaked-profile heating discharges is found (see Fig. 7) to be higher by a factor of 4 when compared to the broad-density profile cases.

We must add that after the pellet-injection, discharge parameters evolve over a relatively long period of time ($\approx$1 s), see Fig. 5, and a steady-state of the enhanced-phase is not fully achieved. In some shots, T_{i0} and R_{DD} decrease even before the T_{e0} crashes due to an MHD event. Poor performance of two peaked-profile discharges (see Fig. 3 and 4) with respect to others is not clearly understood although one of them was heated in the monopole antenna configuration whereas all others were in the dipole mode. The efficiency of ICRH power deposited in the center in the monopole-mode is believed to be generally lower (due to the power lost at the edge) than the dipole mode and may account for its poor performance. Also, attempts were made to plot the data in a way

similar to that shown in Fig. 3 and 4 but, now sorted with the n_e-peaking factor ($n_{e0}/<n_e>$), T_e-peaking factor ($T_{e0}/<T_e>$) and an average η_e-parameter ($T_{e0}/<T_e>$)/($n_{e0}/<n_e>$) but, the results of such an exercise did not reveal any clear dependence on these parametres.

3.0 DISCHARGE SIMULATION ANALYSIS:

3.1 RF Power-Deposition Profiles:

The power-deposition profiles are calculated by the ray-tracing code BRAYCO (Bhatnagar et al, 1984) that self-consistently takes the finite antenna geometry, its full radiation spectrum and the hot-plasma damping into account. The calculation is made at several time slices. For the shot # 16211, out of the total power absorbed, typically, 73 % is given to the minority, 7 % to electrons (electron transit-time magnetic-pumping and Landau-damping) and 20 % to deuterons by second-harmonic. The power density at the second harmonic is relatively small (typically 0.5 W/cc) and using a bounce-average Fokker-Planck ion-cyclotron code BAFIC (Core, 1989; Hamnen et al, 1985), we find that it does not produce strong deuterium tail and thus most of the power is taken-up by the background deuterons. But, the minority produces a relatively strong tail. The time-dependent tail-distribution and the power transfer to the background species has been calculated using the BAFIC code. It is found that for electrons the steady-state is reached in about a Spitzer time τ_s (for definition see, for example, Stix, 1975) and for ions it is much quicker. In the present analysis, for simplicity, we have used the steady-state Stix-model (Stix, 1975). The steady-state calculation overestimates P_e and P_i. Generally, for a relatively constant τ_s, the error would be largest at the start of the RF pulse but, would decrease as time progresses. However, in the present pellet injection shot, τ_s = 30 ms only at t = 43.2 s and increases to 0.6 s at t = 44.2 s. Relative to charateristic time of the variation $\cong$ 0.35 s, the error in calculating P_i is small but, P_e is moderately overestimated. The steady-state RF power delivered to electrons ($P_{e\infty}$) and ions ($P_{i\infty}$) and their profiles calculated by ray-tracing for a peaked-profile discharge are shown in Fig. 8, where the symbol (∞) refers to the steady-state when the minority tail has been fully formed. Note that, due to higher density, a significant fraction of the minority power goes to background ions. Calculations made at a few time slices of this shot are plotted in Fig. 5. Note that initially a larger fraction of power is delivered to ions which is consistent with the rapid rise of T_{i0}. The steady rise of T_e is related to the continuously increasing P_e. In these calculations peaking of T_e, T_i and n_e-profiles is appropriately taken into account. For central heating there is little difference in the (H)-minority power-deposition profile, but, the redistribution of power among electrons and deuterons depends on the local plasma parameters.

3.2 *Transport-Code Simulations :*

We use the Rebut-Lallia model (Rebut et al, 1988) as a reference model in our $1^{1/2}$-D transport code JETTO (Cenacchi and Taroni, 1988) that solves the electron and ion energy-balance equations and the poloidal-field diffusion equation with neo-classical resistivity. The density profiles, the radiated-power profiles and Z_{eff} are taken from the JET experimental data base. The deposition profiles of the RF-power imparted to electrons and ions computed as above are used. An accurate analysis of the discharge requires that both the time evolution of scalar quantities such as stored energy, R_{DD} etc. and profiles of T_e, T_i etc. are correctly simulated. We first note that though the Rebut-Lallia model, in its present form, does not simulate the plasma during the peaked-density phase of the discharge, but it simulates it well after the crash when the peaked-profile is lost. An attempt to simulate the former phase of the discharge is carried out by an adhoc reduction in the values of χ_e and χ_i in the central region (see below). The simulated time evolution of T_e, T_i, $<T_e>$ for shot # 16211 is shown in Fig. 9 which is compared to the corresponding experimental data. The experimental T_i-profile in this shot of ICRF heating alone, was not available as the CXR-spectroscopic diagnostic was inoperative due to the absence of neutral-beam injection. The T_i-profile in this case was assumed to be of the same form as that of T_e. (See below for simulation of another shot where T_i-profile was measured experimentally). To reproduce the time-evolution and the temperature profiles in the 'good confinement-phase' (before the crash) where the density profile is peaked in the central region ($\rho/a < 0.5$), the values of the electron and ion heat-conductivities are both required to be reduced significantly in the inner-half radius (see Fig. 10 (a)) from those that are used to simulate the discharge after the crash. With such a prescription the characteristic profiles of improved confinement are well reproduced as shown in Fig. 10 (b). The temperature profiles after the crash are similar to the standard monster-like discharges and are simulated in the usual way (Taroni et al, 1988) giving good agreement with experimental profiles as shown in Fig. 10(c).

A similar behaviour is found by the analysis of the results of T_e and T_i-profile simultion of another similar pellet-feuled peaked density profile shot # 17749 in which $P_{RF} = 12.5$ MW and we had additional $P_{NBI} = 4.6$ MW. In this case, experimental ion-temperature profiles are available from CXR-spectroscopy. The time evolution of the discharge was roughly similar to that of #16211 as shown in Fig. 5. The discharge was simulated as discussed above. In this case as well, the electron and ion heat-conductivities in the central region are required to be lower as mentioned above and are shown in Fig. 11 (a). A comparison of simulated and experimental T_e and T_i-profiles before the crash (t = 44.15 s; the good confinement phase) and after the crash (t = 44.75 s; after the end of the good confinement phase) are shown in Fig 11 (b) and (c) respectively. We point out that the crash occured at about t = 44.25 s and the RF power was switched-off at t = 44.8 s. Notice that in this shot, even 500 ms after the crash, the T_e and, in particular, the T_i-profiles did not fully relax to the ones typical of a monster sawtooth (as was the case in shot # 16211 shown in Fig. 10). This is, at least in part, the reason for the required strong diminution χ_i at $\rho/a < 0.4$ even after the crash. Further, in this shot large difference in the values of T_e and T_i for $\rho/a > 0.4$ are somewhat puzzling and dictate that χ_i for $\rho/a > 0.4$ are larger than those

in shot #16211 which would not be the case if T_i was closer to T_e. Also, we note that uncertainities in the coefficients χ_e and χ_i in the region ($0 < \rho/a < 0.4$) due to radiation are lower as most of the input power is deposited in the central region whereas the radiation takes place outside. The values of χ_e and χ_i in the region $\rho/a < 0.2$ are prone to large errors particularly in relation to uncertainities in the position of the magnetic axis.

We note that the value of χ_e is reduced but remains strongly anomalous in the region of good confinement ($\chi_{e\,neo} \approx (m_e/m_i)^{1/2} \chi_{i\,neo}$). Further, χ_i is reduced to values roughly close to neoclassical (note that $\chi_{i\,neo} \propto q^2$, thus the uncertainity in q reflects strongly in $\chi_{i\,neo}$). However, all estimates of η_i give rather large values ($\eta_i \geq 3$) even in the good confinement phase (Taroni et al, 1988; Hammett et al, 1989).

4.0 DISCUSSION AND CONCLUSIONS :

In other tokamaks, for example, ASDEX (Gruber et al, 1988), it has been observed that after pellet injection in an ohmic discharge or with counter neutral-beam injection, the density profile peaks (possibly due to increased ratio of inward drift velocity to diffusion). But, the electron temperature profile recovers on a rather short time-scale (2 ms). This leads to η_e and η_i-parameter to fall (and remain) below unity resulting in reduced η_i-driven turbulence which is consistent with the observed improvement in confinement. However, in the JET experiment, peaking of the density profile occurs as in other tokamaks but, the electron temperature profile continues to peak steadily, though, it is broader immediately after the pellet injection. Thus the T_e-profile evolves significantly in defiance of the profile consistency and peaks significantly whereas the density profile peaking dimnishes moderately as a function of time. Such an evolution of T_e and n_e-profiles results in fact that the η_e and η_i-parameter remains below unity only for a short duration (0.2-0.3 s) after the pellet injection and increases steadily (Taroni et al, 1988 ;Hammett et al, 1989) to become as high as 4, although the discharge remains in a good confinement phase in which both the electron and ion heat transport are reduced in the core region. Such a behaviour is inconsistent with the presently available η_i-driven turbulence theories. We must add that in the JET experiment, shortly after the pellet injection, central ICRF heating is applied which ultimately heats electrons and this could be the cause of subsequent significant peaking of the T_e-profile compared to the ASDEX experiment mentioned above. Also, we note that in cases where ICRF heating is significantly delayed after the pellet injection, the η_e-values remain below unity for a correspondingly longer duration and rises thereafter as in other cases.

As mentioned before, the Rebut-Lallia model needs to be improved or completed with other mechanisms in the plasma-core to explain the improvement of confinement self-consistently in the peaked-profile phase of the discharge heated by ICRF. The intense ICRF heating produces a very strong pressure gradient in the proximity of the magnetic-axis and hence produces a significant amount of boot-strap current (Stubberfield et al 1989) which is peaked off-axis. This makes the total plasma current profile hollow and would lead to a q-profile which is non-monotonic over the plasma cross section and the shear (δq / δr) is locally reduced considerably and may even be inverted over a part of the profile. It is conjectured (Rebut et al, 1988) that inclusion of such effects in the Rebut-Lallia model may lead to improved confinement in the central plasma region in the peaked-profile discharges. However, sufficiently accurate evolutions of q-profiles are not yet available to support or reject the idea of strong dependence of transport on the value of shear in the central region.

Using the ray-tracing calculations, we have found that in the (H-minority) in D-majority plasma, significant power ($\approx$20 %) goes to the second-harmonic heating without a strong tail and heats the plasma ions directly which is consistent with the stronger ion heating observed in such discharges. In a (He^3-minority) in D-majority plasma also, strong ion heating was observed although there is no possibility of the second-harmonic heating. In this case we expect again stronger ion heating as the He^3-minority ion tail is relatively weaker (due to its charge and mass) than for the hydrogen-tail and it relaxes more favourably on the background deuterium ions. The transport-code simulation of a He^3-minority discharge has also been carried out and it confirms the improvement of confinement in the central region as in the case of H-minority discharge presented here.

We must point out that the central ion-temperature measured by the Doppler-broadening of the Ni-XXVII impurity line is an underestimate when the electron temperature is greater than about 8.5 KeV and the plasma rotation velocity is negligible. This is related to the ionization-potential of the line and in that case the dominant contribution to the signal is from slightly off-axis and the central temperaturewould be higher. The discharge simulation has also been done by taking this correction into account and the values of χ_i obtained are within the error-bars shown in Fig. 10. Further, there is a relatively large uncertainity on the location of the magnetic-axis from different diagnostics and that obtained from magnetic measurements (plasma equilibrium-calculation code IDENTC at JET) This fact which relates to the calculation of the plasma volume and a lack of accurate knowledge of the deuteron dilution profile leads to a rather large error bars on the discharge simulation values of the neutron production rate.

In conclusion, during the ICRF heating of peaked-density profile in JET limiter discharges, we find typically that T_{i0} is higher roughly by a factor of 2 and T_{e0} roughly by 35 % at a fixed P_{TOT}/n_{e0} when compared to non-peaked profile cases. Also, on a similar comparison, the neutron production rate is found to be higher roughly by a factor of 4. The central confinement improves significantly whereas there is about 20 % improvement in the global electron kinetic-energy confinement. For central heating, the power-deposition profile changes little with the peaking factor but ion heating is improved in the pellet case due to a higher collisionality between the background ions and the energetic minority. Full ray-tracing calculations of power transferred to electrons and ions are consistent with the rate of rise of T_{e0} and T_{i0} in peaked-profile cases. The transport-code simulation of these discharges reveals that there is a reduction of both χ_e and χ_i in the central region of the plasma in the ICRF heated peaked-profile discharges. However, identification of the physical mechanism(s) that play a role in this improvement must await further evaluation.

5.0 ACKNOWLEDGEMENT :

We wish to thank our colleagues in the JET team, especially the RF plant team, joint JET-USDOE pellet group, the tokamak operation team and those operating the diagnostics used in the experiments reported in this paper. Discussions with Drs. M. Bures, G. Hammett, P. Kupschus, S. Milora, G. Schmidt, F. Tibone and M. Watkins are appreciated.

6.0 REFERENCES :

(1) BHATNAGAR V.P. et al, (1984) Nucl. Fusion, 24, 955.
(2) BHATNAGAR V.P. et al (1989a) 16th European Conf. on Controlled Fusion and Plasma Physics, Venice, Italy, Europhysics Conf. Abstracts Vol. 13B, Part I, 127.
(3) BHATNAGAR V.P. et al, (1989b) Plasma Phys. and Contr. Fusion, 31, 333.
(4) CAMPBELL D.J. et al (1988) Phys. Rev. Lett., 60, 2148.
(5) CENACCHI G. and TARONI A.(1988) JET Joint Underataking, Report JET-IR(88)03 (unpublished)
(6) CHRISTIANSEN J.P. et al, Bull. American Phys Society, 33 (1988) 2030.
(7) COPPI B. and SPIGHT C. (1978) Phys. Rev. Lett., 41, 551.
(8) CORE W.G.C. (1989) Private Communication.
(9) DOMINGUEZ R. and WALTZ R.E. (1987) Nucl. Fusion, 27, 65.
(10) FURTH H.P. (1986) Plasma Phys and Contr. Fusion, 28, 9A, 1305.
(11) GOLDSTON R. et al, (1986) Proc. IAEA Conf. on Plasma Physics and Controlled Nuclear Fusion Research, Kyoto, Japan; Nuclear Fusion Supplement 1986, vol. 1, 75.
(12) GREENWALD M. et al (1984) Phys. Rev. Lett., 53, 352.
(13) GRUBER O. et al, (1988) Plasma Phys Contr. Fusion, 30, 1611.
(14) HAMMETT G.W. et al (1989) 16th European Conf. on Controlled Fusion and Plasma Physics, Venice, Italy, Europhysics Conf. Abstracts Vol. 13B, Part I, 131.
(15) HAMNEN H. et al, (1985) JET Joint Undertaking, Report JET-DN-T(85)23 (unpublished).
(16) HORTON W. (1981) Physics Fluids, 24, 1077.
(17) JACQUINOT J. et al, (1988) Plasma Phys and Contr. Fusion, 30, 1467.
(18) JACQUINOT, J. et al (1986) Proc. IAEA Conf. on Plasma Phys. and Contr. Nuclear Fusion Research, Kyoto, Japan, Nuclear Fusion Supplement 1987, vol. 1, 449.
(19) KAYE A.S. et al (1987) Fusion Technology, 2, 203.
(20) KUPSCHUS P. et al (1988) 15th European Conf. on Controlled Fusion and Plasma Physics, Dubrovnik, Yogoslavia, Europhysics Conf. Abstracts Vol. 12B, Part I, 143.
(21) LEE C.S. and DIAMOND P.H. (1986) Nucl. Fusion, 29, 3291.
(22) MILORA S.L. et al (1988) 15th European Conf. on Controlled Fusion and Plasma Physics, Dubrovnik, Yogoslavia, Europhysics Conf. Abstracts Vol. 12B, Part I, 147.
(23) MILORA S.L. et al (1989) 16th European Conf. on Controlled Fusion and Plasma Physics, Venice, Italy, Europhysics Conf. Abstracts Vol. 13B, Part I, 91.
(24) ORLINSKIJ D.V. and MAGYAR G. (1988) Nucl. Fusion, 28, 611.
(25) PEGORARO F. et al, (1988) Proc. IAEA Conf. on Plasma Physics and Controlled Nuclear Fusion Research, Nice, France, paper CN-50/D-4-6.

(26) REBUT P.H. et al, (1984) Proc. IAEA Conf. on Plasma Physics and Controlled Nuclear Fusion Research, London, England, Nuclear Fusion supplement 1985, vol. 1, 11.
(27) REBUT P.H. et al, (1988) Proc. IAEA Conf. on Plasma Physics and Controlled Nuclear Fusion Research, Nice, France, paper CN-50/D-4-1.
(28) ROMANELLI F. et al (1986) Nucl. Fusion, 26, 1515.
(29) ROMANELLI F. and BRIGUGLIO S. (1988) Plasma Phys and Contr. Fusion (to be published)
(30) SCHMIDT G. et al, (1988) Proc. IAEA Conf. on Plasma Physics and Controlled Nuclear Fusion Research, Nice, France, paper CN-50/A-4-1.
(31) STIX T.H. (1975) Nucl. Fusion, 15, 737.
(32) STUBBERFIELD P.M. et al (1989) 16th European Conf. on Controlled Fusion and Plasma Physics, Venice, Italy, Europhysics Conf. Abstracts Vol. 13B, Part IV, 1255.
(33) TARONI A. et al, (1988), Proc. IAEA Conf. on Plasma Physics and Controlled Nuclear Fusion Research, Nice, France, paper CN-50/A-7-1.
(34) WADE T. et al (1985) Proc. 11th Symposium on Fusion Engineering, Austin, Texas.
(35) WHITE, R. et al, (1988), Phys. Rev. Letters, 60, 2038.

TABLE 1. RANGE OF JET PLASMA PARAMETERS UNDER ICRF HEATING

WITH AND WITHOUT PELLET PEAKED-PROFILE

Item	Without pellet	With pellet
ICRH Power (MW)	0 - 16	0 - 13
RF Frequency (MHz)	25 - 52	32 - 48
Toroidal Field (T)	2 - 3.5	3.1 - 3.3
Plasma Current (MA)	1 - 6	3 - 3.3
OH Power (MW)	0.7 - 4.5	2.5 - 3
Average Plasma Density (m^{-3})	$2 - 5 \times 10^{19}$	$4 - 6 \times 10^{19}$
Central Electron Temperature (keV)	2 - 10	5 - 12
Central Ion Temperature (keV)	2 - 7.5	5 - 10
Plasma Effective Charge	2 - 5	2 - 4

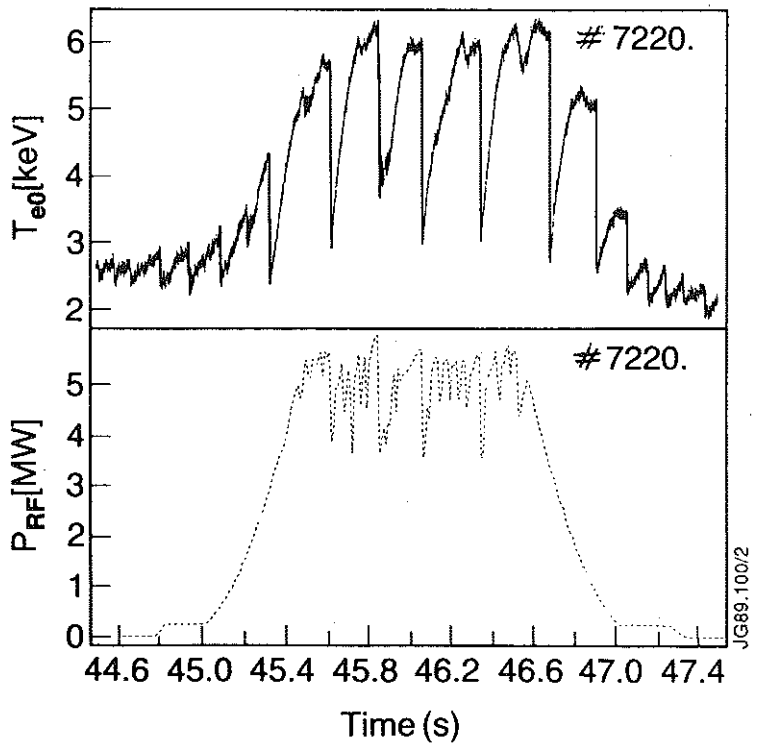

FIG. 1. The giant sawteeth activity in JET with increased amplitude and period of sawteeth during ICRH (I_p = 2 MA, q_ψ = 6)

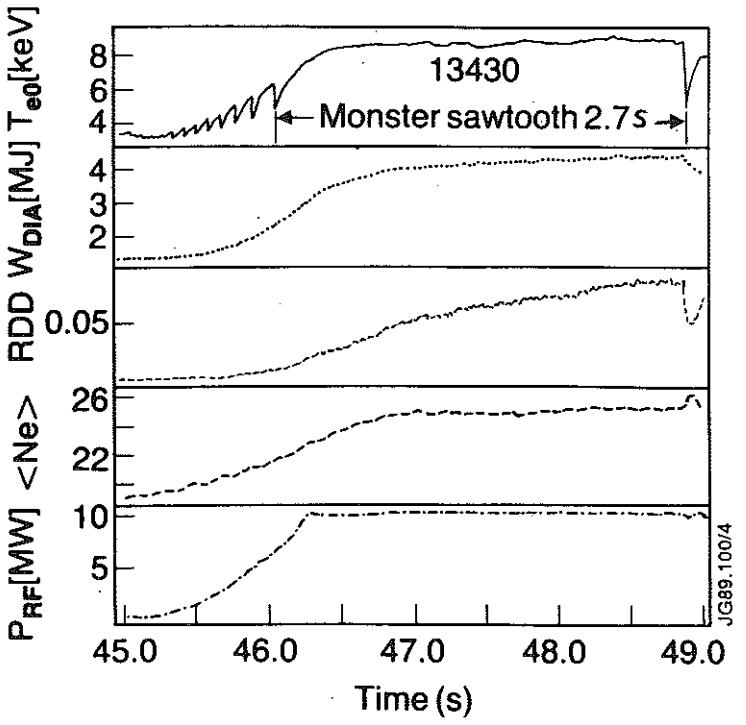

FIG. 2. A characteristic "monster" sawtooth JET discharge with sawtooth stablization by minority ICRF Heating.

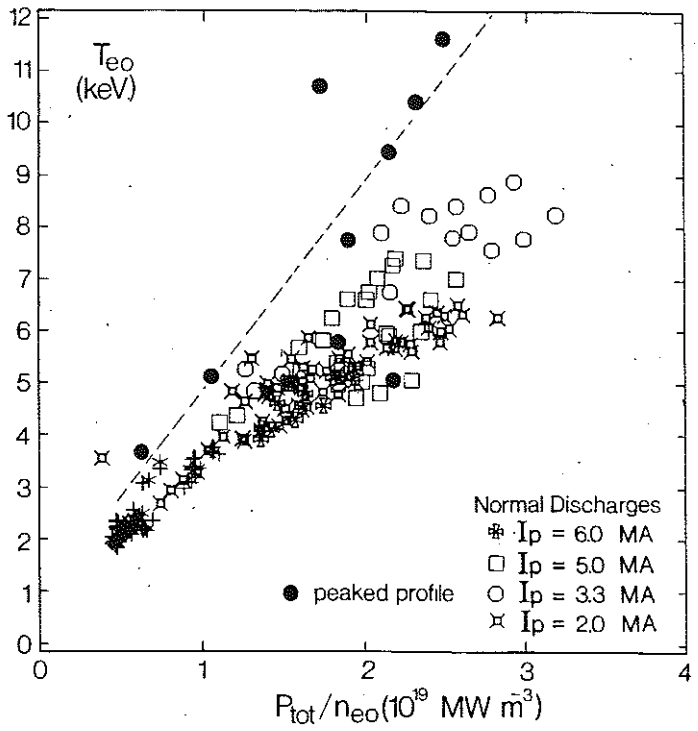

FIG. 3. A plot of T_{e0} vs P_{tot}/n_{e0} for peaked profile and normal discharges. Macroscopic data analysis does not reveal any insight as to why two peaked-profile shots performed poorly.

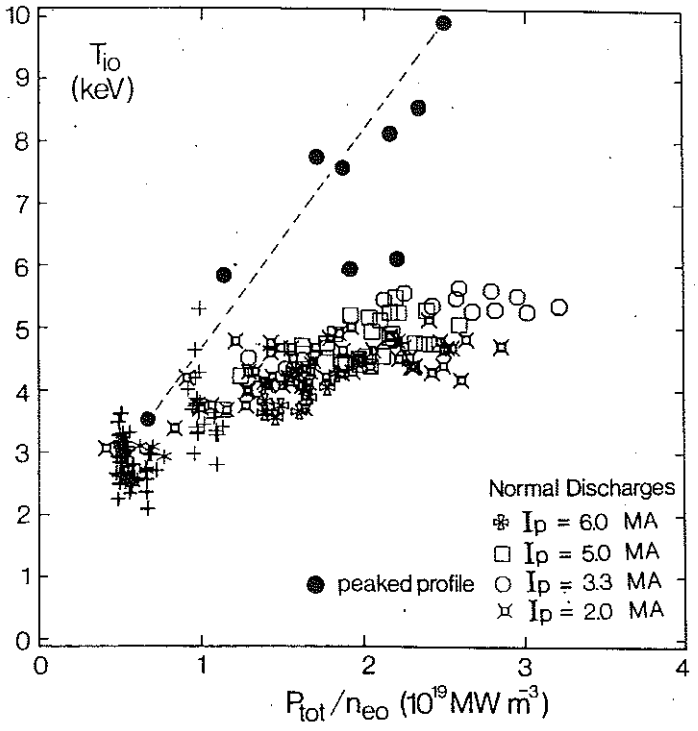

FIG. 4. A plot of T_{i0} vs P_{tot}/n_{e0} for peaked profile and normal discharges. See remark in Fig. 3.

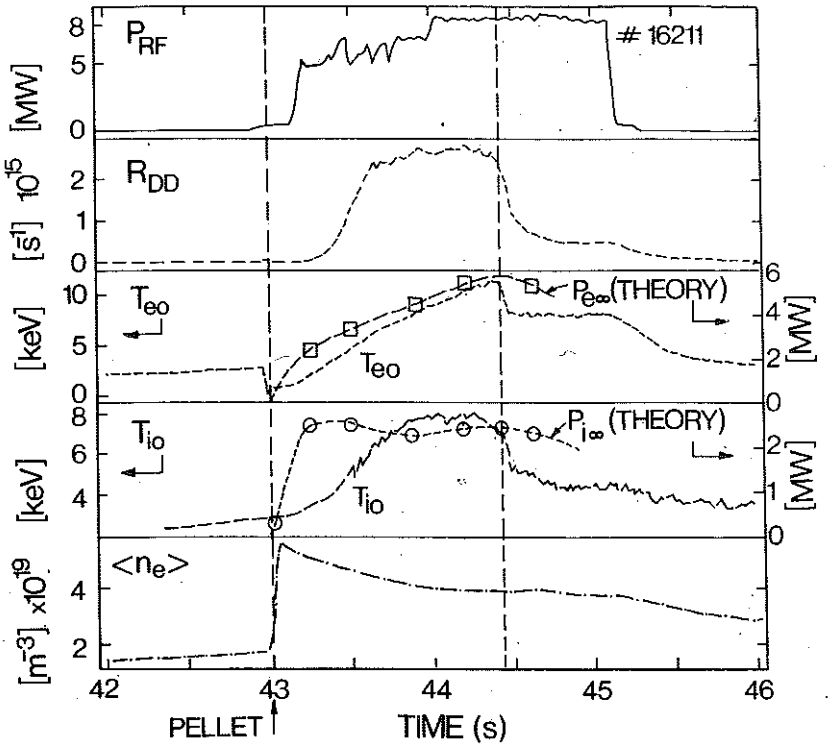

FIG. 5. Time traces of P_{RF}, R_{DD}, T_{e0}, T_{i0} and $< n_e >$ in a pellet produced peaked density profile discharge. Theory refers to ray-tracing calculations.

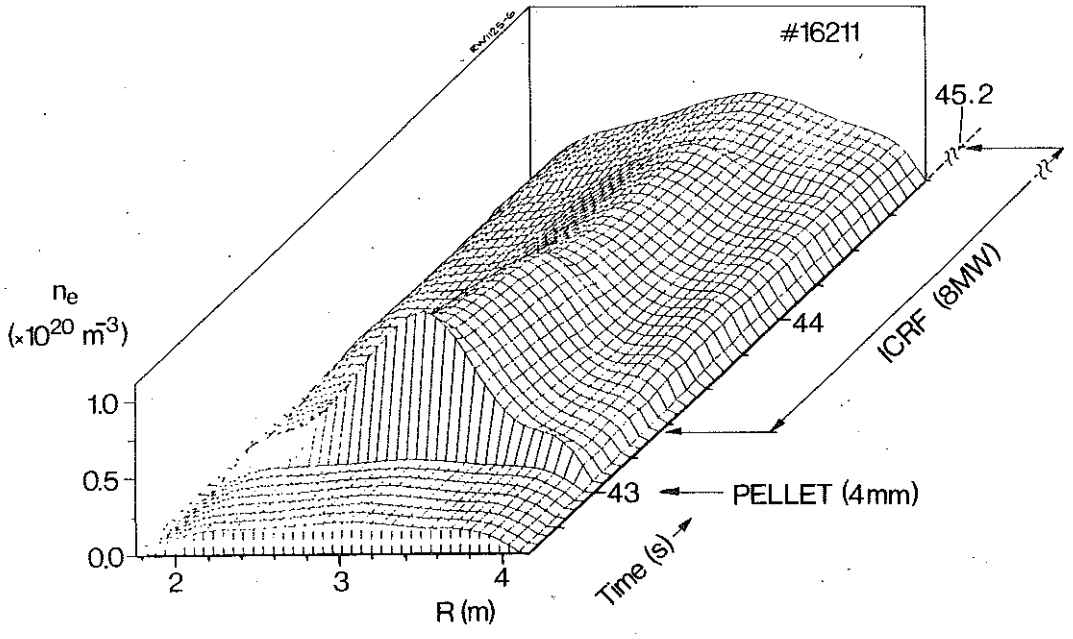

FIG. 6 A 3-dimensional plot of the evolution (as a function of time) of electron-density profile over the plasma cross section obtained by Abel-inversion of the line-density measured by interferometric diagnostics.

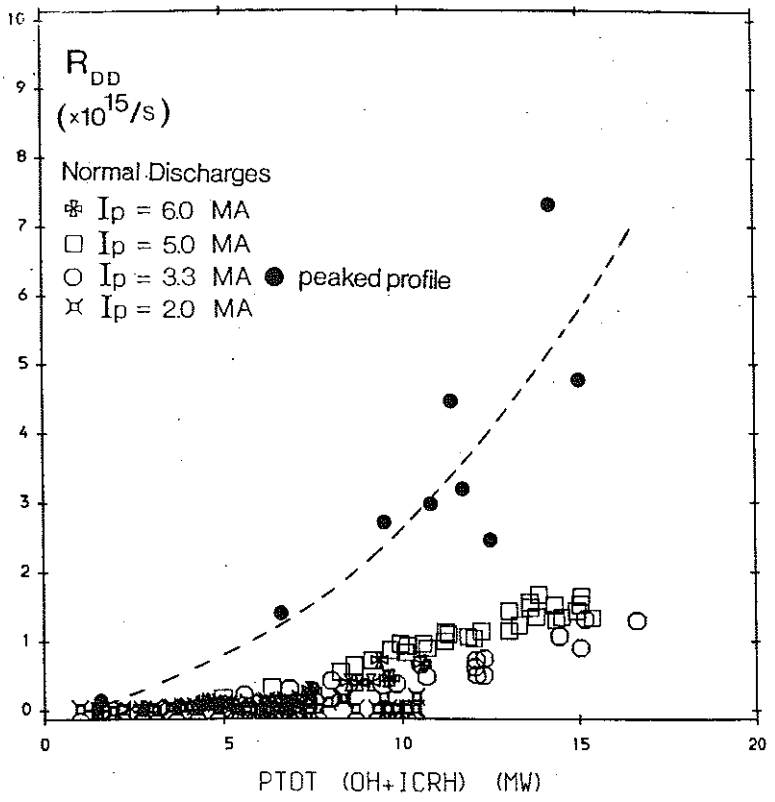

FIG. 7 A plot of D-D reaction rates vs. total input power for peaked profile and normal discharges.

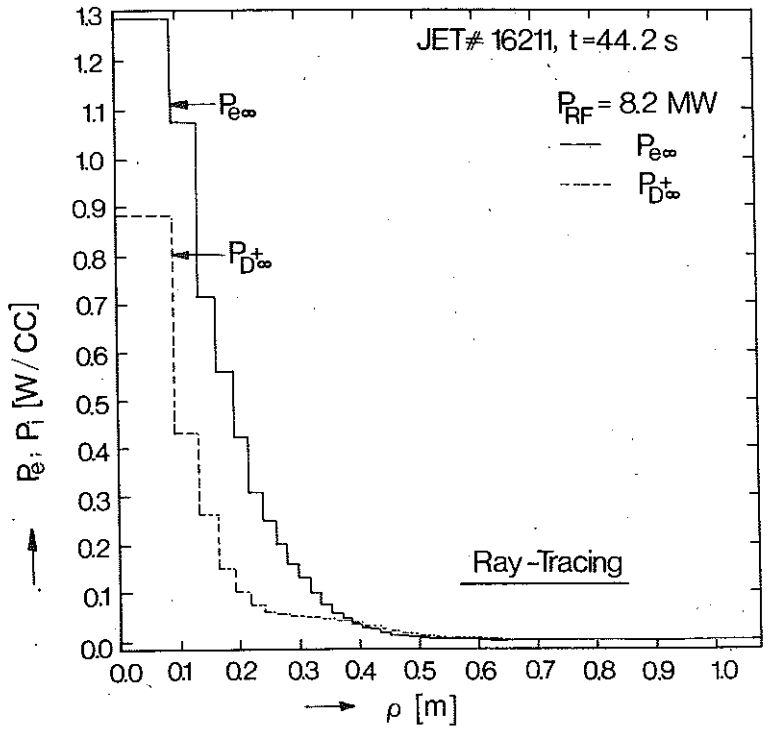

FIG. 8. Steady-state power-deposition profile of elctrons and ions produced by ray-tracing. The minority species was hydrogen and n_H / n_D was taken to be 0.03.

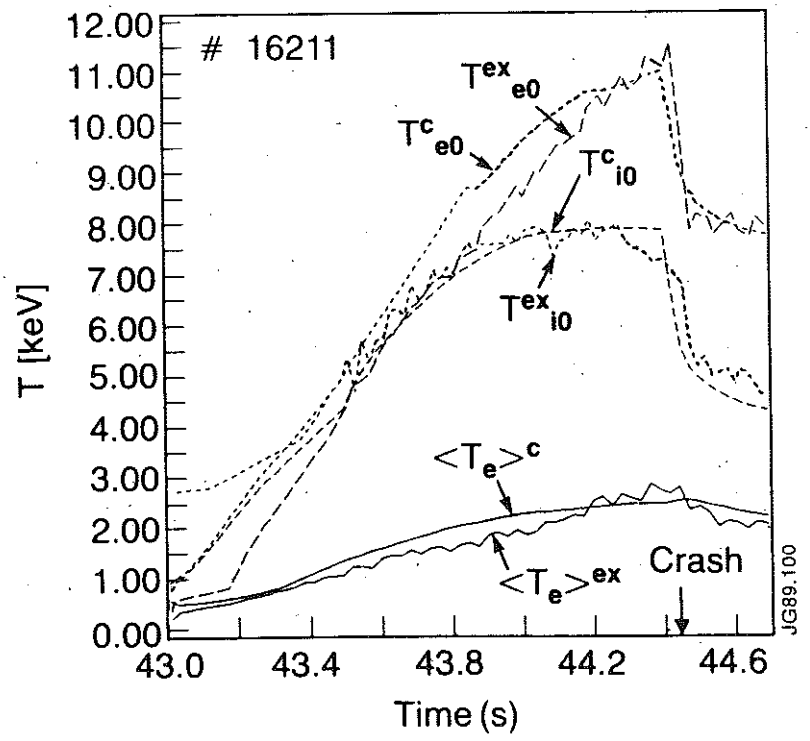

FIG. 9 A comparison of the computed (c) and experimental (ex) central electron (T_{e0}) and ion (T_{i0}) temperatures and volume average electron temperature ($<T_e>$) time evolution for a pellet peaked-profile JET discharge.

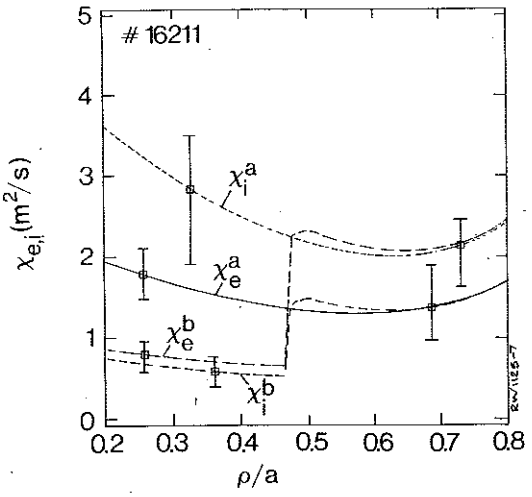

FIG. 10 (a) The profiles of χ_e and χ_i that are used to simulate the shot # 16211 before (t = 44.3 s) and after (t = 44.7 s) the crash. The x-axis is a normalized plasma radial distance ρ/a in this and the following figures.

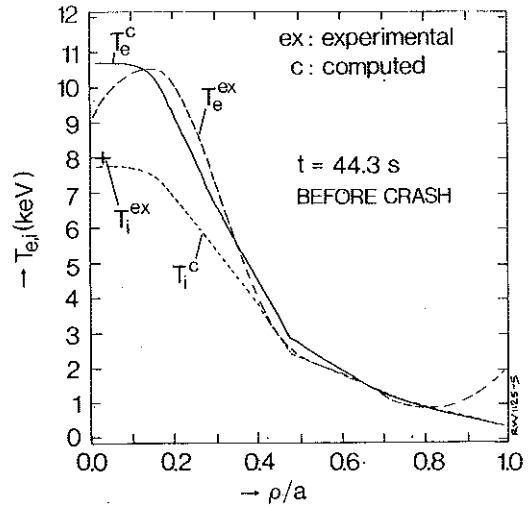

FIG. 10 (b) Experimental and computed temperature profiles before the crash for shot #16211.

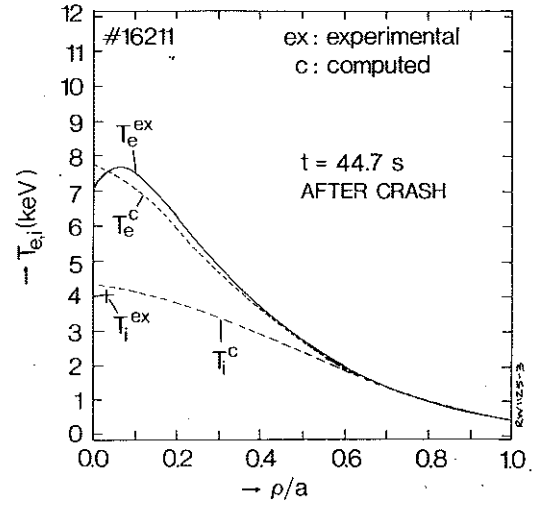

FIG. 10 (c) Experimental and computed temperature profiles after the crash for shot # 16211.

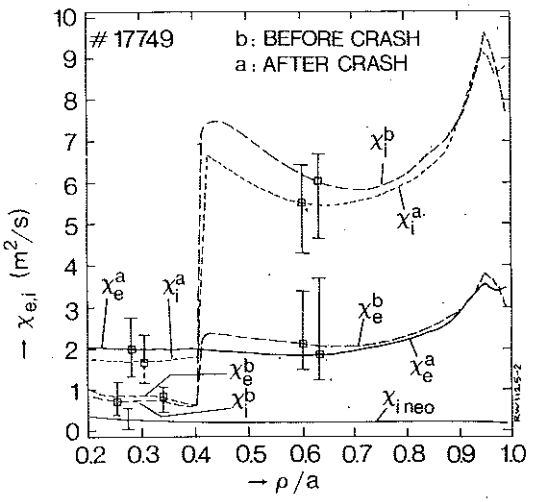

FIG. 11 (a) The profiles of χ_e and χ_i that are used to simulate the shot # 17749 before (t = 44.15 s) and after (t = 44.75 s) the crash. The neoclassical heat-conductivity $\chi_{i\,neo}$ which is practically the same for the two time-slices considered is also given.

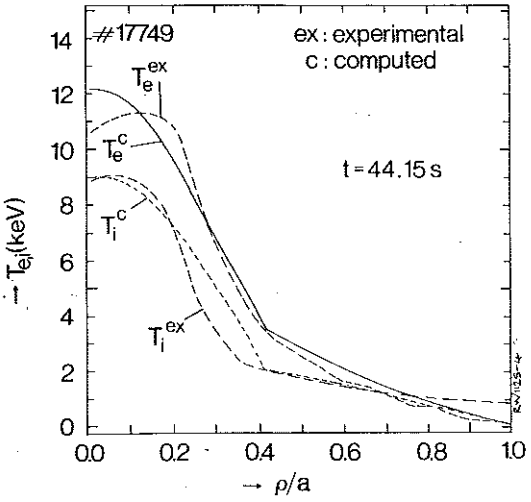

FIG. 11 (b) Experimental and computed temperature profiles before the crash for shot # 17749.

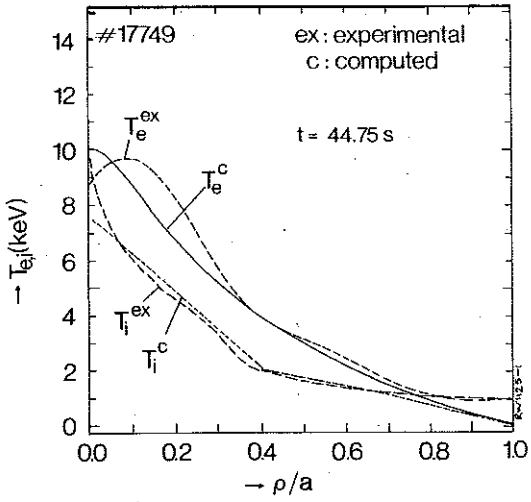

FIG. 11 (c) Experimental and computed temperature profiles after the crash for shot # 17749.

APPENDIX 1.

THE JET TEAM

JET Joint Undertaking, Abingdon, Oxon, OX14 3EA, U.K.

J.M.Adams[1], F.Alladio[4], H.Altmann, R.J.Anderson, G.Appruzzese, W.Bailey, B.Balet, D.V.Bartlett, L.R.Baylor[24], K.Behringer, A.C.Bell, P.Bertoldi, E.Bertolini, V.Bhatnagar, R.J.Bickerton, A.Boileau[3], T.Bonicelli, S.J.Booth, G.Bosia, M.Botman, D.Boyd[31], H.Brelen, H.Brinkschulte, M.Brusati, T.Budd, M.Bures, T.Businaro[4], H.Buttgereit, D.Cacaut, C.Caldwell-Nichols, D.J.Campbell, P.Card, J.Carwardine, G.Celentano, P.Chabert[27], C.D.Challis, A.Cheetham, J.Christiansen, C.Christodoulopoulos, P.Chuilon, R.Claesen, S.Clement[30], J.P.Coad, P.Colestock[6], S.Conroy[13], M.Cooke, S.Cooper, J.G.Cordey, W.Core, S.Corti, A.E.Costley, G.Cottrell, M.Cox[7], P.Cripwell[13], F.Crisanti[4], D.Cross, H.de Blank[16], J.de Haas[16], L.de Kock, E.Deksnis, G.B.Denne, G.Deschamps, G.Devillars, K.J.Dietz, J.Dobbing, S.E.Dorling, P.G.Doyle, D.F.Düchs, H.Duquenoy, A.Edwards, J.Ehrenberg[14], T.Elevant[12], W.Engelhardt, S.K.Erents[7], L.G.Eriksonn[5], M.Evrard[2], H.Falter, D.Flory, M.Forrest[7], C.Froger, K.Fullard, M.Gadeberg[11], A.Galetsas, R.Galvao[8], A.Gibson, R.D.Gill, A.Gondhalekar, C.Gordon, G.Gorini, C.Gormezano, N.A.Gottardi, C.Gowers, B.J.Green, F.S.Griph, M.Gryzinski[26], R.Haange, G.Hammett[6], W.Han[9], C.J.Hancock, P.J.Harbour, N.C.Hawkes[7], P.Haynes[7], T.Hellsten, J.L.Hemmerich, R.Hemsworth, R.F.Herzog, K.Hirsch[14], J.Hoekzema, W.A.Houlberg[24], J.How, M.Huart, A.Hubbard, T.P.Hughes[32], M.Hugon, M.Huguet, J.Jacquinot, O.N.Jarvis, T.C.Jernigan[24], E.Joffrin, E.M.Jones, L.P.D.F.Jones, T.T.C.Jones, J.Källne, A.Kaye, B.E.Keen, M.Keilhacker, G.J.Kelly, A.Khare[15], S.Knowlton, A.Konstantellos, M.Kovanen[21], P.Kupschus, P.Lallia, J.R.Last, L.Lauro-Taroni, M.Laux[33], K.Lawson[7], E.Lazzaro, M.Lennholm, X.Litaudon, P.Lomas, M.Lorentz-Gottardi[2], C.Lowry, G.Magyar, D.Maisonnier, M.Malacarne, V.Marchese, P.Massmann, L.McCarthy[28], G.McCracken[7], P.Mendonca, P.Meriguet, P.Micozzi[4], S.F.Mills, P.Millward, S.L.Milora[24], A.Moissonnier, P.L.Mondino, D.Moreau[17], P.Morgan, H.Morsi[14], G.Murphy, M.F.Nave, M.Newman, L.Nickesson, P.Nielsen, P.Noll, W.Obert, D.O'Brien, J.O'Rourke, M.G.Pacco-Düchs, M.Pain, S.Papastergiou, D.Pasini[20], M.Paume[27], N.Peacock[7], D.Pearson[13], F.Pegoraro, M.Pick, S.Pitcher[7], J.Plancoulaine, J-P.Poffé, F.Porcelli, R.Prentice, T.Raimondi, J.Ramette[17], J.M.Rax[27], C.Raymond, P-H.Rebut, J.Removille, F.Rimini, D.Robinson[7], A.Rolfe, R.T.Ross, L.Rossi, G.Rupprecht[14], R.Rushton, P.Rutter, H.C.Sack, G.Sadler, N.Salmon[13], H.Salzmann[14], A.Santagiustina, D.Schissel[25], P.H.Schild, M.Schmid, G.Schmidt[6], R.L.Shaw, A.Sibley, R.Simonini, J.Sips[16], P.Smeulders, J.Snipes, S.Sommers, L.Sonnerup, K.Sonnenberg, M.Stamp, P.Stangeby[19], D.Start, C.A.Steed, D.Stork, P.E.Stott, T.E.Stringer, D.Stubberfield, T.Sugie[18], D.Summers, H.Summers[20], J.Taboda-Duarte[22], J.Tagle[30], H.Tamnen, A.Tanga, A.Taroni, C.Tebaldi[23], A.Tesini, P.R.Thomas, E.Thompson, K.Thomsen[11], P.Trevalion, M.Tschudin, B.Tubbing, K.Uchino[29], E.Usselmann, H.van der Beken, M.von Hellermann, T.Wade, C.Walker, B.A.Wallander, M.Walravens, K.Walter, D.Ward, M.L.Watkins, J.Wesson, D.H.Wheeler, J.Wilks, U.Willen[12], D.Wilson, T.Winkel, C.Woodward, M.Wykes, I.D.Young, L.Zannelli, M.Zarnstorff[6], D.Zasche[14], J.W.Zwart.

PERMANENT ADDRESS

1. UKAEA, Harwell, Oxon. UK.
2. EUR-EB Association, LPP-ERM/KMS, B-1040 Brussels, Belgium.
3. Institute National des Récherches Scientifique, Quebec, Canada.
4. ENEA-CENTRO Di Frascati, I-00044 Frascati, Roma, Italy.
5. Chalmers University of Technology, Göteborg, Sweden.
6. Princeton Plasma Physics Laboratory, New Jersey, USA.
7. UKAEA Culham Laboratory, Abingdon, Oxon. UK.
8. Plasma Physics Laboratory, Space Research Institute, Sao José dos Campos, Brazil.
9. Institute of Mathematics, University of Oxford, UK.
10. CRPP/EPFL, 21 Avenue des Bains, CH-1007 Lausanne, Switzerland.
11. Risø National Laboratory, DK-4000 Roskilde, Denmark.
12. Swedish Energy Research Commission, S-10072 Stockholm, Sweden.
13. Imperial College of Science and Technology, University of London, UK.
14. Max Planck Institut für Plasmaphysik, D-8046 Garching bei München, FRG.
15. Institute for Plasma Research, Gandhinagar Bhat Gujat, India.
16. FOM Instituut voor Plasmafysica, 3430 Be Nieuwegein, The Netherlands.
17. Commissiariat à L'Energie Atomique, F-92260 Fontenay-aux-Roses, France.
18. JAERI, Tokai Research Establishment, Tokai-Mura, Naka-Gun, Japan.
19. Institute for Aerospace Studies, University of Toronto, Downsview, Ontario, Canada.
20. University of Strathclyde, Glasgow, G4 ONG, U.K.
21. Nuclear Engineering Laboratory, Lapeenranta University, Finland.
22. JNICT, Lisboa, Portugal.
23. Department of Mathematics, Univeristy of Bologna, Italy.
24. Oak Ridge National Laboratory, Oak Ridge, Tenn., USA.
25. G.A. Technologies, San Diego, California, USA.
26. Institute for Nuclear Studies, Swierk, Poland.
27. Commissiariat à l'Energie Atomique, Cadarache, France.
28. School of Physical Sciences, Flinders University of South Australia, South Australia SO42.
29. Kyushi University, Kasagu Fukuoka, Japan.
30. Centro de Investigaciones Energeticas Medioambientales y Techalogicas, Spain.
31. University of Maryland, College Park, Maryland, USA.
32. University of Essex, Colchester, UK.
33. Akademie de Wissenschaften, Berlin, DDR.

CR 88.49.1A